


Quantum graph wave external triggering: Energy transfer and dampingF. Plouraboué *Institut de Mécanique des Fluides de Toulouse (IMFT), Université de Toulouse, CNRS, INPT, UPS, Toulouse, France*

(Received 23 September 2023; accepted 19 February 2024; published 20 May 2024)

The propagation of wave trains resulting from a local external trigger inside a network described by a metric graph is analyzed using quantum graph theory. The external trigger is a finite-time perturbation imposed at one vertex of the graph, leading to a consecutive wave train into the network, supposedly at rest before the applied external perturbation. A complete analytical solution for the induced wave train is found having a specific spectrum as well as mode's amplitudes. Furthermore the precise condition by which the external trigger can transfer a maximal energy to any specific natural mode of the quantum graph is derived. Finally, the wave damping associated with boundary-layer dissipation is computed within a multiple time-scale asymptotic analysis. Exponential damping rates are explicitly found related to their corresponding mode's eigenvalue. Each mode energy is then obtained, as well as their exponential damping rate. The relevance of these results to the physics of waves within networks are discussed.

DOI: [10.1103/PhysRevE.109.054310](https://doi.org/10.1103/PhysRevE.109.054310)**I. INTRODUCTION**

First introduced for the study of chemical vibrations spectrum arising in molecules by Pauling [1], the concept of quantum graphs associated with Schrödinger equation defined along each one-dimensional coupled chemical bounds has since then been developed in many areas and contexts [2,3]. Quantum graphs now cover operators equipping a metric graph, i.e., a graph whose edges have a physical length. The broadening of the quantum graph concept has thus enlarged the physical fields and related issues associated with it. From coupled vibrations and spectrum structure in metric graphs [4], quantum chaos, e.g., Refs. [5,6], wave scattering [7,8], more recent interests have been focused on wave propagation within them, e.g., Ref. [9]. Recent advances in various physical domains such as magnons propagation in magnetoelectric materials [10], cavity magnonics [11], surface polaritons [12], microwave networks [13–17], nanophotonics [18,19] are interested in waves in networks having wirelike connections. Furthermore in more traditional engineering areas such as water-hammer waves in pipelines [20] or pulse pressure waves in vascular beds [21] this issue is also important. The wavelength of the waves are in every case much larger than the size of the wirelike substrate so that a one-dimensional propagation model is relevant within each individual wirelike substrate (e.g., branch, vessel, cavity, pipe, fiber, chemical bound, etc.) of the network, so that a one-dimensional wave operator—a long-wavelength approximation—is relevant for these waves propagation and interaction. In these contexts, there are technological motivations to control, manipulate, or refill the energy of confined sustained waves. This is, for example, done by the use of injection seeders in nanophotonics or spin current injection in spin-wave propagation [22]. In this case one needs to open the network in order to inject some energy into it [23]. Also, the opposite can occur during a possibly unintentional opening of the network,

where some energy loss could occur. This is, for example, the case for water-hammer generation within pipe's networks generally produced by network management events (valve's sudden opening or closure, pipe breakdown, pump's shut-down, etc.) [24]. In these contexts it is interesting to consider how a sudden, finite-time event arising at a given location might perturb and/or generate a wave train propagating inside the network. This issue has been previously addressed many times in the engineering community with the use of numerical simulations where the network edges have to be finely discretized (cf. Ref. [25] and references therein). On the contrary to these numerical discrete approaches, a quantum graph formulation permits a spectral discretization of the wave solution along each network's edge saving a huge numerical cost [26]. Furthermore, quantum graph theory permits us to establish general results, which numerical computations can only illustrate. In this contribution transient wave propagation resulting from external trigger within metric graphs is theoretically analyzed. Both undamped and damped propagation are considered. Damped wave propagation in metric graph has received attention from the mathematical viewpoint, since certain class of damping models lead to non-self-adjoint operators [27]. In this contribution we analyze small damping effect resulting from a well-established acoustic and fluid-mechanics boundary layer damping within a perturbation approach. This damping model does not modify the self-adjointness of the Laplacian operator on the metric graph.

Section II introduces the wave model under consideration as well as quantum graph theory. Section III discusses the undamped wave propagation resulting from an external trigger. Section IV describes how the external trigger can be shaped in order to maximize the energy transfer into internal modes. Section V discuss the wave damping resulting from a time-delayed damping model. The physical relevance and significance of the obtained theoretical results are discussed in Sec. VII.

II. THEORETICAL FRAMEWORK

A. Damped waves propagation model

We consider a wave moving at constant wave speed c_p within a complex network. Rescaling the time t^* by the time for a unit length to be covered by the wave $t_1 = 1/c_p$ defines a dimensionless time $t = t^*/t_1 = c_p t^*$ for which inside each wirelike connection, equipped with axial coordinate x , the pressure p fulfills the dimensionless damped wave propagation problem [21]

$$\left(\frac{\partial^2}{\partial t} - \frac{\partial^2}{\partial x^2} \right) p = 2\epsilon \frac{\partial \tau_w}{\partial x}, \quad (1)$$

where τ_w is the wall shear rate, and where ϵ is a small parameter. In the context of acoustic or fluid mechanics, this small parameter ϵ is called the water-hammer dimensionless number [20,21]. It is built upon the time-scale ratio between the longitudinal time scale for the wave to propagate within the network L/c_p , to the radial diffusion of the wave within the boundary layer R^2/ν (where ν is the fluid kinematic viscosity, R the pipe radius), i.e., $\epsilon = \nu L/R^2 c_p$. In many applications, associated to blood hammer, or water hammer $\epsilon \ll 1$ [20,21]. For example, for a propagating distance of $L = 10^4$ m, for water $\nu = 10^{-6}$, within a pipe radius $R = 10^{-1}$ m, in steel material where $c_p \approx 10^3$ m/s, which are realistic parameters for water distribution networks, $\epsilon \approx 10^{-3}$. Hence, in the following an asymptotic solution of (1) within a metric graph is searched for. The wall-shear rate is related to the longitudinal velocity gradient within the boundary layer [21,28]. Solving for the velocity field radial variation within the boundary layer, leads to a relation with the longitudinal pressure gradient [21,28]

$$\tau_w = -\frac{1}{\sqrt{\pi}} \int_0^t \frac{1}{\sqrt{t-t'}} \frac{\partial p(t')}{\partial x} dt', \quad (2)$$

which is nonlocal in time (due to the time-delayed response of the boundary layer), and involves the convolution product of the pressure gradient with the diffusion kernel. As found in Ref. [28], in Laplace domain using variable s conjugate to time, the Laplace transform $\tilde{\tau}_w$ of τ_w (2) reads (cf. Appendix A 1 for more information)

$$\tilde{\tau}_w = -\frac{1}{\sqrt{s}} \frac{\partial \tilde{p}(s, x)}{\partial x}. \quad (3)$$

Hence, the damped wave propagation problem (1) is a nonlocal problem in time, the solution of which is not straightforward. This is why a considerable literature has been devoted to solve it numerically, e.g., Refs. [20,29]. One interesting alternative approach first introduced in Ref. [21] is to benefit from its perturbed nature, i.e., using the fact that the damping term is $O(\epsilon)$ small and search for a multi-time-scale solution. At leading order, for fast time, the damping is neglected as detailed in Sec. III. At first order one can compute the long-time scale corrections resulting from the influence of the damping term and establish the damping rates as detailed in Sec. V.

B. Quantum graph theory for Laplacian eigenfunctions and spectrum on metric graphs

We consider an undirected compact metric graph $\mathcal{G}(\mathcal{V}, \mathcal{E})$, having vertex set \mathcal{V} and edge one \mathcal{E} the cardinal of which are, respectively, denoted V and E . The corresponding undirected nonmetric graph is denoted G . \mathcal{G} (and G) are not multigraphs, i.e., there is a single edge connecting two distinct vertices, and contain no vertex with self-edges. The connection mapping between the vertex set is provided by the adjacency $V \times V$ symmetric matrix \mathbf{A} (as \mathcal{G} is undirected), both for \mathcal{G} and G . On this metric graph \mathcal{G} continuous function Ψ along finite (since \mathcal{G} is compact) metric edges $e_k \in \mathcal{E}$ being intervals $[0, \ell_{ij} \equiv \ell_{e_k}]$ (with $i, j \in [1, V]$) the vertex indexes joined by edge e_k are considered in the H^2 Sobolev space over \mathcal{G} denoted $\mathcal{H}_{\mathcal{G}}$

$$\mathcal{H}_{\mathcal{G}} \equiv H^2(\mathcal{G}) = \bigoplus_{e_k \in \mathcal{E}} H^2(e_k). \quad (4)$$

Laplacian operator over \mathcal{G} denoted $-\Delta_{\mathcal{G}}$ and acting over $\Psi \in \mathcal{H}_{\mathcal{G}}$ is defined as the operator $-\frac{d^2}{dx^2}$ with $x \in [0, \ell_{e_k}]$ lying along each edge $e_k \in \mathcal{E}$ equipped at each vertex with one of the following vertex conditions:

(1) Kirchhoff condition (also called natural or current conservation [30]) meaning continuity of Ψ and that the sum of the normal derivatives of Ψ at vertex is zero,

(2) Dirichlet condition meaning continuity of Ψ at vertex whereas a prescribed value $\Psi = 0$ is also imposed there,

(3) Kirchhoff-Robin condition meaning continuity of Ψ and that the sum of the normal derivatives of Ψ at vertex is proportional to the value of Ψ at vertex.

Is it possible to show that condition (iii) can be degenerated into (i) or (ii) [31], this is why, in the following, (iii) is considered as a general formulation. Furthermore it is known that $-\Delta_{\mathcal{G}}$ is a self-adjoint and semibounded operator [32]. Its spectrum consists of a sequence of real eigenvalues of finite multiplicity, and it admits an orthogonal base of eigenfunctions. Following Refs. [2,26], one considers the eigenfunctions $\Psi_{\lambda} \in \mathcal{H}_{\mathcal{G}}$ of $-\Delta_{\mathcal{G}}$ whose values between vertex i and j along straight metric edge e_{ij} of length ℓ_{ij} traveled along distance x (being zero at vertex i) are denoted $\Psi_{ij}(x)$. Ψ_{λ} can be viewed as a E -component vector of functions $\Psi_{ij}(x)$, with, again $i, j \in [1, V]$ being the vertex indexes joined by edge e_k . The restriction of Ψ_{λ} over \mathcal{V} , i.e., $\Psi_{\lambda}|_{\mathcal{V}}$ defines a V -component vector denoted ϕ_{λ} having ϕ_j amplitudes with $j \in [1, V]$. Along each edge the component $\Psi_{ij}(x)$ of the solution Ψ_{λ} is a solution of

$$-\frac{d^2}{dx^2} \Psi_{ij}(x) = \lambda^2 \Psi_{ij}(x). \quad (5)$$

Dirichlet continuity at vertex i and j reads

$$\Psi_{ij}(0) = \phi_i \quad \Psi_{ij}(\ell_{ij}) = \phi_j. \quad (6)$$

Denoting A_{ij} the components of \mathbf{A} , the Neumann continuity condition at each vertex i reads

$$-\sum_{j<i} A_{ij} \frac{d}{dx} \Psi_{ij}(\ell_{ij}) + \sum_{j>i} A_{ij} \frac{d}{dx} \Psi_{ij}(0) = h_i \phi_i. \quad (7)$$

Condition (7) is Kirchhoff-Robin condition (iii). For $h_i = 0$ it degenerates to Kirchhoff condition (i). On the contrary, in

the limit $h_i \rightarrow \infty$, it gives a Dirichlet condition (ii) at vertex i where it imposes $\phi_i = 0$. Given the continuity conditions (6) $\Psi_{ij}(x)$ can be adequately chosen, without loss of generality, as

$$\Psi_{ij}(x) = \frac{A_{i,j}}{\sin(\lambda \ell_{ij})} \{ \phi_i \sin[\lambda(\ell_{ij} - x)] + \phi_j \sin(\lambda x) \}. \quad (8)$$

(8) is built to have by construction, a unique continuous value across each vertices satisfying the continuity condition (6), as well as the Laplacian equation (5). (8) is a spectral base for the wave propagation solution, the precision of which converges exponentially with the number of modes [26]. It is interesting to note that if λ and ϕ_λ are known, Ψ_λ is analytically defined on G from (8), so that numerically, ϕ_λ and λ are equivalent to Ψ_λ .

Furthermore the Kirchhoff-Robin condition (7) used at each vertex i leads to

$$h_i \phi_i = - \sum_{j < i} \frac{\lambda A_{ij}}{\sin(k \ell_{ij})} [-\phi_j + \phi_i \cos(\lambda \ell_{ij})] + \sum_{j > i} \frac{\lambda A_{ij}}{\sin(k \ell_{ij})} [-\phi_i \cos(\lambda \ell_{ij}) + \phi_j]. \quad (9)$$

(9) defines a set of linear homogeneous equations for the ϕ_i amplitudes of Ψ_λ over vertices. Hence a $V \times V$ symmetric matrix \mathfrak{A} defined as

$$\mathfrak{A}_{ij}(\lambda, \mathbf{h}) = -\delta_{ij} \left(\sum_{m \in \mathfrak{N}(i)} A_{im} \cot(\lambda \ell_{im}) + \frac{h_i}{\lambda} \right) + A_{ij} \frac{1}{\sin(\lambda \ell_{ij})}, \quad (10)$$

where $\mathfrak{N}(i) = \{m \mid A_{im} \neq 0\}$ being the neighbor vertices of vertex i associated with nonzero components of adjacency matrix \mathbf{A} . Matrix \mathfrak{A} , sometimes called the secular matrix, is built so that (9) is equivalent to

$$\sum_{j=1}^V \mathfrak{A}_{ij} \phi_j = \mathfrak{A} \phi_\lambda = 0, \quad (11)$$

where, again, ϕ_λ is the V -component vector of amplitudes ϕ_j . (11) can have a nontrivial solution different from zero when the so-called secular condition is met

$$\det \mathfrak{A}(\lambda, \mathbf{h}) = 0. \quad (12)$$

The secular condition can be interpreted as finding the solution within the kernel of the $\mathfrak{A}(\lambda)$ matrix, which encapsulates the boundary conditions at any vertex. It generalizes to a metric graph how the spectrum within a single pipe is found from connecting boundary conditions with transfer matrix [33]. Condition (12) provides the condition defining the discrete eigenvalues set of the Laplacian operator subsequently denoted λ_n . Several other approaches can be used to find a similar secularity condition, e.g., scattering approach over edges [2] or mixed vertex and edges approaches [34]. Since each matrix entry $\mathfrak{A}_{ij}(\lambda)$ (10) of matrix \mathfrak{A} is Lipschitz

continuous, so does $\det \mathfrak{A}(\lambda)$. Furthermore since $\lambda \in \mathbb{R}$, i.e., lying in one dimension, provided that $d[\det \mathfrak{A}(\lambda)]/d\lambda \neq 0$, the implicit-function theorem states that $\lambda_n(\ell_{e_{ij}}, h_i)$ is a single-value function of parameters $\ell_{e_{ij}}$ with $e_{ij} \in \mathcal{E}$ and h_i (if h_i is chosen to be either zero or infinity there are only E parameters $\ell_{e_{ij}}$), so that each λ_n has algebraic multiplicity one. This implies that the null space of $\mathfrak{A}(\lambda_n)$ is one-dimensional, i.e., $\forall n \in \mathbb{N}$, $\dim \text{Ker} \mathfrak{A}(\lambda_n) = 1$.

When $h_i = 0, \forall i \in [1, V]$, i.e., $\mathbf{h} = \mathbf{0}$, then it is known that the minimum eigenvalue of the discrete spectrum $\lambda_1 = 0$ being associated with a constant eigenfunction Ψ_{λ_1} . On the contrary if $\exists i \in [1, V]$ such that $h_i \neq 0$, then $\lambda_1 \neq 0$ and Ψ_{λ_1} is not constant over \mathcal{G} [34]. This paper focuses on Kirchhoff vertex where $h_i = 0$ or Dirichlet ones where $h_i \rightarrow \infty$ of relation (1) where constant pressure boundary conditions are imposed. It is nevertheless interesting to note that condition (iii) has also been considered to model leakage within pipes [35,36] (when the transient wave pressure amplitude is small compared to the steady static one), so that the considered framework and related approach is also relevant to analyze leaking pipe's networks. $\mathcal{V}_K \subset \mathcal{V}$ and its complement subset $\mathcal{V}_D \subset \mathcal{V}$, respectively, denote the subsets of \mathcal{V} where Kirchhoff or Dirichlet conditions are applied such that $\mathcal{V}_K \cup \mathcal{V}_D = \mathcal{V}$ and $\mathcal{V}_K \cap \mathcal{V}_D = \emptyset$. It is interesting to mention that the spectral properties of $\Delta_{\mathcal{G}}$ are unchanged when adding a new Kirchhoff two-degree vertex within any edge of \mathcal{G} [2,32] (gluing a dummy Kirchhoff vertex as described in Ref. [32]).

In the following, a supplementary nonhomogeneous condition is applied at one of the Kirchhoff vertexes denoted $v_O \in \mathcal{V}_K$ called the origin vertex for wave generation. Multiple origins could also be considered, receiving a similar treatment as subsequently provided, but to avoid unnecessary complexity, a single origin is chosen. This origin vertex v_O is the location of the sudden change in boundary condition. In the context of pressure waves within pipe's networks it is associated with the sudden opening or closure of a valve or a pipe breakage at a given location leading to a surge, i.e., a water-hammer bouncing waves all around into the pipe's network modeled as a metric graph \mathcal{G} [24].

The spectrum of discrete eigenvalue λ_n of the operator $\Delta_{\mathcal{G}}$ has to be complemented by their corresponding eigenfunctions Ψ_{λ_n} . We introduce notation $\Psi_{ij}^n(x) \equiv \Psi_{e_k}^n(x)$ for the k th component function of Ψ_{λ_n} , being a E -component vector of functions defined over each edge $k \in [1, E]$ joining vertices i and j . But, as previously mentioned, Ψ_{λ_n} is equivalent to the datum of λ_n and ϕ_{λ_n} . Given λ_n , only ϕ_{λ_n} has then to be computed to find Ψ_{λ_n} . Condition (11) implies that vector $\phi_{\lambda_n} \subset \text{Ker} \mathfrak{A}(\lambda_n, \mathbf{h})$. Hence, ϕ_{λ_n} can be computed using standard algebraic techniques to obtain the eigenvectors spanning the null space of $\mathfrak{A}(\lambda_n, \mathbf{h})$ [26]. Finally, in order to find the base orthogonality, one has to define the scalar product between the distinct (i.e., $n \neq m$) eigenfunctions Ψ_{λ_n} and Ψ_{λ_m}

$$\langle \Psi_{\lambda_n}, \Psi_{\lambda_m} \rangle = \sum_{e_k \equiv e_{ij} \in \mathcal{E}} \int_0^{\ell_{ij}} \Psi_{ij}^n \Psi_{ij}^m dx. \quad (13)$$

Using (8), in (13) one finds

$$\begin{aligned} \langle \Psi_{\lambda_n}, \Psi_{\lambda_m} \rangle &= \sum_{e_k \equiv e_{ij}} \left((\phi_i^n \phi_j^m + \phi_j^n \phi_i^m) [-\lambda_n \cot(\lambda_n \ell_{ij}) + \lambda_m \cot(\lambda_m \ell_{ij})] \right. \\ &\quad \left. - (\phi_i^n \phi_j^m + \phi_j^n \phi_i^m) \left(\frac{\lambda_n}{\sin(\lambda_n \ell_{ij})} - \frac{\lambda_m}{\sin(\lambda_m \ell_{ij})} \right) \right) \frac{A_{ij}}{(\lambda_n^2 - \lambda_m^2)}. \end{aligned} \quad (14)$$

Realizing that the sum over the vertex set is twice the sum over edge set (since there is only one edge connecting two vertices) since each edge is visited twice, (14) can be rewritten as half the same sum over vertices. Introducing notations $\mathfrak{A}^n = \mathfrak{A}(\lambda_n, \mathbf{h})$ as well as \mathbf{D}^n and \mathbf{A}^n the matrices derived from (10)

$$D_{ij}^n = -\delta_{ij} \left(\sum_{m \in \mathcal{V}(i)} A_{im} \cot(\lambda_n \ell_{im}) + \frac{h_i}{\lambda} \right), \quad (15)$$

$$A_{ij}^n = A_{ij} \frac{1}{\sin(\lambda_n \ell_{ij})}, \quad (16)$$

such that $\mathfrak{A}^n = \mathbf{D}^n + \mathbf{A}^n$ one can then rewrite (14) as

$$\langle \Psi_{\lambda_n}, \Psi_{\lambda_m} \rangle = \frac{1}{4} \sum_{j=1}^V \sum_{i=1}^V (-\lambda_n \phi_i^n (D_{ij}^n + A_{ij}^n) \phi_j^m + \lambda_m \phi_i^m (D_{ij}^m + A_{ij}^m) \phi_j^n) \frac{1}{(\lambda_n^2 - \lambda_m^2)}, \quad (17)$$

so that finally, expressing (17) as a compact matrix-vector contraction (a quadratic form) while using (11) leads to the orthogonality for $n \neq m$

$$\langle \Psi_{\lambda_n}, \Psi_{\lambda_m} \rangle = \frac{1}{4} \frac{(-\lambda_n \phi_{\lambda_m} \mathfrak{A}^n \phi_{\lambda_n} + \lambda_m \phi_{\lambda_n} \mathfrak{A}^m \phi_{\lambda_m})}{(\lambda_n^2 - \lambda_m^2)} = 0, \quad (18)$$

where Einstein's convention for repeated index has been used. For $n = m$ the scalar product (13) using (8) simplifies to

$$\langle \Psi_{\lambda_n}, \Psi_{\lambda_n} \rangle = \sum_{e_k \equiv e_{ij}} \left((\phi_i^n \phi_j^n + \phi_j^n \phi_i^n) \left(-\cot(\lambda_n \ell_{ij}) + \frac{\lambda_n \ell_{ij}}{\sin^2(\lambda_n \ell_{ij})} \right) + 2\phi_i^n \phi_j^n \left(-\frac{1}{\sin(\lambda_n \ell_{ij})} + \lambda_n \ell_{ij} \frac{\cot(\lambda_n \ell_{ij})}{\sin(\lambda_n \ell_{ij})} \right) \right) \frac{A_{ij}}{2\lambda_n}. \quad (19)$$

Since (19) is a scalar equality, and since each eigenvector ϕ_{λ_n} having components ϕ_i^n $i \in [1, V]$ that are all defined [in the one-dimensional null space of $\mathfrak{A}(\lambda_n)$] up to a scaling multiplying factor μ_n , this multiplying factor can be chosen so that (19) is unity, i.e., given a set of admissible value for ϕ_i^n , they should be all multiplied by μ_n defined as

$$\frac{1}{\mu_n^2} = \sum_{e_k \equiv e_{ij}} \left((\phi_i^n \phi_j^n + \phi_j^n \phi_i^n) \left[-\cot(\lambda_n \ell_{ij}) + \frac{\lambda_n \ell_{ij}}{\sin^2(\lambda_n \ell_{ij})} \right] + 2\phi_i^n \phi_j^n \left[\frac{1}{\sin(\lambda_n \ell_{ij})} - \lambda_n \ell_{ij} \frac{\cot(\lambda_n \ell_{ij})}{\sin(\lambda_n \ell_{ij})} \right] \right) \frac{A_{ij}}{2\lambda_n}. \quad (20)$$

III. WAVE PROPAGATION ON METRIC GRAPH TRIGGERED FROM AN ORIGIN EVENT

Let us now consider the undamped pressure solution over \mathcal{G} , denoted $\mathbf{P}_G^0 \in \mathcal{H}_G$ being decomposed into a E -component vector of functions $p_k^0(x, t)$ defined along each metric edge $e_k \in \mathcal{E}$ bounded by vertices i and j . The wave propagation problem (1) without damping (i.e., when $\epsilon = 0$) within each edge reads

$$\left(\frac{\partial^2}{\partial \tau^2} - \frac{\partial^2}{\partial x^2} \right) p_k^0(x, \tau) = 0 \quad (21)$$

or more compactly, the leading-order problem for \mathbf{P}_G^0 is

$$\left(\frac{\partial^2}{\partial \tau^2} - \Delta_{\mathcal{G}} \right) \mathbf{P}_G^0 \equiv -\square \mathbf{P}_G^0 = 0. \quad (22)$$

A time-domain solution $\mathbf{P}_G^0 \in \mathcal{H}_G$ for the leading-order solution is obtained from separable variable decomposition over

the Laplacian $\Delta_{\mathcal{G}}$'s eigenfunctions Ψ_{λ_n}

$$\begin{aligned} \mathbf{P}_G^0 &= \sum_{n \in \mathbb{N}} (A_n(T) a_n e^{i\lambda_n \tau} + A_n(T)^* a_n^* e^{-i\lambda_n \tau}) \Psi_{\lambda_n} + \mathbf{P}_p \\ \mathbf{P}_G^0 &= \sum_{n \in \mathbb{N}} (A_n(T) a_n e^{i\lambda_n \tau} + \text{c.c.}) \Psi_{\lambda_n} + \mathbf{P}_p, \end{aligned} \quad (23)$$

with long-time T defined as $T = \epsilon \tau$ and its associated long-time complex amplitude $A_n(T)$ multiplying each mode, where \star denotes complex conjugate. In (23) c.c. stands for the complex-conjugate expression of the term within parenthesis. In the sequel we refer to the first term of right-hand side of (23) as the homogeneous part of \mathbf{P}_G^0 whereas the second term \mathbf{P}_p is called its particular part. The spectrum of the homogeneous part is built from previously defined secular matrix $\mathfrak{A}(\lambda, \mathbf{0})$ chosen such as $\forall v_i \in \mathcal{V}, i \in [1, V], h_{v_i} \equiv h_i = 0$ in (10), with zero determinant condition (12). Since the eigenfunctions Ψ_{λ_n} satisfy Dirichlet boundary conditions over \mathcal{V}_D and Kirchhoff ones over \mathcal{V}_K so does the pressure field \mathbf{P}_G^0 .

The homogeneous component of (23), by construction lies within the null space of $\square_{\mathcal{G}}^{\prime}$ operator and fulfills (22). In the early stage of the propagation the fast-time τ being $O(1)$, then $T \sim O(\epsilon)$ so that

$$A_n(T) = A_n(\epsilon\tau) \approx A_n(0) \quad \tau \ll O(1/\epsilon), \quad T \ll 1. \quad (24)$$

Condition (24) provides a validity condition for the leading-order solution to hold. A normalization condition is then set on $A_n(T)$ so that the long-time scale is an asymptotic perturbation of the leading-order solution

$$A_n(0) = 1. \quad (25)$$

In Sec. III $\mathbf{P}_{\mathcal{G}}^0$ is computed in the limit $\epsilon \rightarrow 0$ for early-stage fast-time τ satisfying condition (24) so that $A_n = 1$ here. Furthermore, the pressure field fulfills an additional non-homogeneous time-dependent imposed boundary condition at the origin vertex v_O , located at \mathbf{x}_{v_O} , which needs to be added. This condition is associated with an added flux within each pipe connected to the origin vertex and depending on time [33]. Since the flux is related to the local pressure gradient along each pipe direction, the condition reads

$$\sum_{e_k} \frac{\partial \mathbf{P}_{\mathcal{G}}^0}{\partial x}(\mathbf{x}_{v_O}, \tau) = P_O(\tau), \quad (26)$$

where $P_O(t)$ is supposed to be a $[0, T_e]$ compact support, square integrable L^2 function over the analyzed period T_e . Defining $\tau_e < T_e$ as the typical duration time of the triggering, during the recording finite interval $[0, T_e]$ there is no constraint concerning the relative value of τ_e compared to the typical propagation time L/c_p built over the typical length L . Nevertheless, it is interesting to have in mind that τ_e could be smaller than L/c_p for the excitation time to be short compared to the wave propagation inside the network. $P_O(t)$ is sometimes called the closure law in water-hammer problems. From linearity, standard Green's functions techniques apply and the impulse response associated with $P_O(t) = \delta(t)$ provides the general solution by convolution with it (δ denotes the Dirac distribution). In the following we keep with a general unspecified closure law $P_O(t)$ and derive a general solution depending on it. We suppose that the origin vertex belongs to the Kirchhoff set, i.e., $v_O \in \mathcal{V}_K$. This is mathematically consistent since a flux condition can not be imposed at the location where another imposed Dirichlet condition has to be met, and physically meaning full since this is where water-hammer events can be triggered. The leading-order solution for the wave pressure propagation (23) within early-time condition (24) simplifies to

$$\mathbf{P}_{\mathcal{G}}^0 = \sum_{n \in \mathbb{N}} (a_n e^{i\lambda_n \tau} + \text{c.c.}) \Psi_{\lambda_n} + \mathbf{P}_p, \quad (27)$$

where the particular solution $\mathbf{P}_p \in \mathcal{H}_{\mathcal{G}}$ takes care of the non-homogeneous condition prescribed at the origin vertex v_O . Since \mathbf{P}_p does not share a Kirchhoff condition on vertex v_O it does not lie inside the image of the Laplace operator $\Delta_{\mathcal{G}}$, so that it can not be fully decomposed into its eigenfunction basis Ψ_{λ_n} . Nevertheless, let us now consider the new self-adjoint Laplacian operator associated with a Kirchhoff-Robin condition at vertex v_O with $h_{v_O} \neq 0$ rather than Kirchhoff one, with all other conditions unchanged on every other vertices,

and denote this operator $\Delta_{\mathcal{G}}^p$. Then, from Kirchhoff-Robin condition (9) with h_{v_O} the eigenmodes $\Psi_{\lambda_n^p}$ of the $\Delta_{\mathcal{G}}^p$ thus verified $\forall n \in \mathbb{N}$

$$\sum_{e_k} \frac{\partial \Psi_{\lambda_n^p}}{\partial x}(\mathbf{x}_{v_O}) = h_{v_O} \Psi_{\lambda_n^p}(\mathbf{x}_{v_O}). \quad (28)$$

$\Delta_{\mathcal{G}}^p$ has a distinct spectrum from $\Delta_{\mathcal{G}}$ since from changing one vertex boundary condition only we change the associated matrix (10), such that secular condition (12) is distinct from the $\Delta_{\mathcal{G}}^{\prime}$ s one. More explicitly, one can define from (10) a distinct matrix $\mathfrak{A}^p(\lambda, \mathbf{h})$ from previous one $\mathfrak{A}(\lambda, \mathbf{0})$, such that for $v_O \in \mathcal{V}$, $h_{v_O} \neq 0$ (yet unspecified, but further defined precisely) and for $\forall v_i \neq v_O \in \mathcal{V}$, $h_{v_i} = 0$, resulting in a distinct spectrum, associated with zero determinant condition (12). By definition, \mathbf{P}_p is part of the operator $\Delta_{\mathcal{G}}^p$ image. One can thus chose \mathbf{P}_p in the null space of $\frac{\partial^2}{\partial \tau^2} - \Delta_{\mathcal{G}}^p \equiv -\square_{\mathcal{G}}^p$ operator, so that, as the homogeneous part the particular solution reads

$$\mathbf{P}_p = \sum_{m \in \mathbb{N}} (A_m^p a_m^p e^{i\lambda_m^p \tau} + \text{c.c.}) \Psi_{\lambda_m^p}. \quad (29)$$

Since the aim of the particular solution is to handle the time variations of the triggering at location \mathbf{x}_{v_O} , rather than choosing $\Psi_{\lambda_m^p}$ as a spatial base, it is more appropriate to chose it as a temporal one. (35) can be set as a temporal base if λ_m^p maps into a Fourier mode series, given the finite recording time T_e (since the triggering has compact support in $[0, T_e]$), $\lambda_m^p = m\pi/T_e$. Hence, each temporal mode λ_m^p define a single $h_{v_O} = h_m$ such as the secularity condition is met, i.e.,

$$\det \mathfrak{A}(\lambda_m^p, \mathbf{h} \equiv h_m \hat{\mathbf{e}}^O) = 0, \quad (30)$$

where $\hat{\mathbf{e}}^O$ is the unit vector of \mathcal{V} on vertex v_O , whose components are $\hat{\mathbf{e}}_i^O = \delta_{i v_O}$. $\Psi_{\lambda_m^p}^p$ then represents a set of nonorthogonal eigenvectors, acting as a forcing term upon the orthogonal base solution decomposed into the base Ψ_{λ_n} . In the sequel, modes $\Psi_{\lambda_m^p}^p$ are referred to as Kirchhoff-Robin-Fourier modes. Similarly as for the homogeneous solution, the same short-time normalization, reads

$$\forall m \in \mathbb{N}, A_m^p(T) \approx A_m^p(0) \quad \tau \ll O(1/\epsilon), \quad T \ll 1, \quad (31)$$

so that at this early-stage fast-time τ satisfying condition (24) $A_m^p = 1$. Using (28) in (26) then leads to

$$\sum_{m \in \mathbb{N}} (a_m^p e^{i\lambda_m^p \tau} + \text{c.c.}) h_m \Psi_{\lambda_m^p}^p(\mathbf{x}_{v_O}) = P_O(\tau). \quad (32)$$

Considering \mathbf{P}_{Om} the real Fourier decomposition coefficients of compact support function \mathbf{P}_O over $[0, T_e]$ interval, given by

$$\mathbf{P}_{Om} = \frac{2}{T_e} \int_0^{T_e} P_O(\tau) \sin m \frac{\pi \tau}{T_e} d\tau. \quad (33)$$

Since $\lambda_m^p = m\pi/T_e$ are precisely the Fourier mode of the particular solution, projecting (32) over each Fourier mode, considering that $(a_m^p e^{i\lambda_m^p \tau} + \text{c.c.}) = 2[\Re(a_m^p) \cos(\lambda_m^p \tau) - \Im(a_m^p) \sin(\lambda_m^p \tau)]$ leads to pure imaginary a_m^p coefficient

reading

$$a_m^p = -\frac{i}{2} \frac{P_{Om}}{h_m} \frac{1}{\Psi_{\lambda_m^p}^p(\mathbf{x}_{v_o})}, \quad (34)$$

which gives the amplitude of vector \mathbf{a}^p by which the particular solution \mathbf{P}_p is achieved. Being purely imaginary,

$$\begin{aligned} \mathbf{P}_p &= -\sum_{m \in \mathbb{N}} A_m^p 2\Im(a_m^p) \sin \lambda_m^p \tau \Psi_{\lambda_m^p}^p \\ &= \sum_{m \in \mathbb{N}} A_m^p \frac{P_{Om}}{h_m} \frac{1}{\Psi_{\lambda_m^p}^p(\mathbf{x}_{v_o})} \sin \lambda_m^p \tau \Psi_{\lambda_m^p}^p. \end{aligned} \quad (35)$$

Now considering the initial condition at rest, such that $\forall \mathbf{x} \neq \mathbf{x}_{v_o}$

$$\mathbf{P}_{\mathcal{G}}^0|_{\tau=0} = 0, \quad \left. \frac{\partial \mathbf{P}_{\mathcal{G}}^0}{\partial t} \right|_{\tau=0} = 0, \quad (36)$$

then permits us to find the modes amplitude a_n , since from (27), while using (35) in (36) one finds that $\forall \mathbf{x} \neq \mathbf{x}_{v_o}$

$$\begin{aligned} \sum_{n \in \mathbb{N}} (a_n + a_n^*) \Psi_{\lambda_n} + \sum_{m \in \mathbb{N}} (a_m^p + a_m^{p*}) \Psi_{\lambda_m^p} &= 0, \\ \sum_{n \in \mathbb{N}} \lambda_n (a_n - a_n^*) \Psi_{\lambda_n} + \sum_{m \in \mathbb{N}} \lambda_m^p (a_m^p - a_m^{p*}) \Psi_{\lambda_m^p} &= 0. \end{aligned} \quad (37)$$

Let us define the projections matrices between eigenfunction base Ψ_{λ_n} and eigenfunctions $\Psi_{\lambda_m^p}$, as

$$\mathbf{\Pi}_{nm} = \langle \Psi_{\lambda_n}, \Psi_{\lambda_m^p}^p \rangle, \quad \mathbf{\Pi}'_{nm} = \frac{\lambda_m^p}{\lambda_n} \mathbf{\Pi}_{nm}, \quad (38)$$

as well as projections matrix between nonorthogonal eigenfunctions $\Psi_{\lambda_m^p}$ and $\Psi_{\lambda_{m'}^p}$

$$\mathbf{\Pi}_{mm'}^{pp} = \langle \Psi_{\lambda_m^p}, \Psi_{\lambda_{m'}^p}^p \rangle, \quad (39)$$

with normalized condition of unit diagonal, i.e., $\mathbf{\Pi}_{mm}^{pp} = 1 \forall m \in \mathbb{N}$. Using the orthogonality of eigenfunctions Ψ_{λ_n}

such that $\langle \Psi_{\lambda_n}, \Psi_{\lambda_{n'}} \rangle = \delta_{nn'}$, (37) then leads to

$$\mathbf{a} = -\frac{1}{2}(\mathbf{\Pi}' + \mathbf{\Pi})\mathbf{a}^p + \frac{1}{2}(\mathbf{\Pi}' - \mathbf{\Pi})\mathbf{a}^{p*}. \quad (40)$$

Furthermore since from (34) \mathbf{a}^p is purely imaginary, so does \mathbf{a} , hence (40) simplifies to

$$\mathbf{a} = -\mathbf{\Pi}'\mathbf{a}^p. \quad (41)$$

(41) then provides an explicit solution for $\mathbf{P}_{\mathcal{G}}^0$ defined in (27) using (35).

IV. SHAPING INTERNAL MODES FROM EXTERNAL TRIGGER

We now consider the physical interpretation of the solution obtained in the previous section and discuss how can it serves interesting physical control of the vibrating modes. First, one should realize that the two right-hand-side terms decomposition of (27) are distinct. The first one, called the homogeneous solution in the previous section (from the corresponding associated boundary condition) decompose the propagating wave into the stationary internal standing wave of the metric graph, which acts as a complex cavity into which only some typical modes of excitations are permitted, which we have denoted Ψ_{λ_n} . The second term decomposes itself into distinct modes, depending specifically on the location of an externally imposed time-varying trigger. This is why the resulting wave denoted \mathbf{P}_p can be considered as a consecutive wave echo of the external trigger. One important specificity about the considered metric graph is that \mathbf{P}_p can not be chosen in the kernel of the metric graph Laplacian since, this kernel is empty. In the case of simple cavities, such as a one-dimensional cavity, on the contrary, the particular solution is found inside the kernel of the Laplacian, triggering no external wave into the cavity [33]. This understood leads to further interesting questions. First, how much energy is produced by the external trigger into internal modes?

A. Wave energy

The triggered wave potential energy is given by

$$\begin{aligned} \frac{1}{2} \overline{\langle \mathbf{P}_{\mathcal{G}}^0, \mathbf{P}_{\mathcal{G}}^0 \rangle} &= \frac{1}{2} \sum_{n, n' \in \mathbb{N}} \overline{(a_n e^{i\lambda_n t} + a_n^{p*} e^{-i\lambda_n t})(a_{n'}^p e^{i\lambda_{n'} t} + a_{n'}^{p*} e^{-i\lambda_{n'} t})} \langle \Psi_{\lambda_n}, \Psi_{\lambda_{n'}} \rangle \\ &\quad + \frac{1}{2} \sum_{n, m \in \mathbb{N}} \overline{(a_n e^{i\lambda_n t} + a_n^{p*} e^{-i\lambda_n t})(a_m^p e^{i\lambda_m^p t} + a_m^{p*} e^{-i\lambda_m^p t})} \langle \Psi_{\lambda_n}, \Psi_{\lambda_m^p}^p \rangle \\ &\quad + \frac{1}{2} \sum_{m, m' \in \mathbb{N}} \overline{(a_m^p e^{i\lambda_m^p t} + a_m^{p*} e^{-i\lambda_m^p t})(a_{m'}^p e^{i\lambda_{m'}^p t} + a_{m'}^{p*} e^{-i\lambda_{m'}^p t})} \langle \Psi_{\lambda_m^p}^p, \Psi_{\lambda_{m'}^p}^p \rangle, \end{aligned} \quad (42)$$

where notation $\overline{f(t)g(t)} = \lim_{T_a \rightarrow \infty} \frac{1}{T_a} \int_0^{T_a} f(\tau)g(\tau)d\tau$ has been used. From time averaging, and eigenmodes orthogonality this potential energy simplifies to

$$\frac{1}{2} \overline{\langle \mathbf{P}_{\mathcal{G}}^0, \mathbf{P}_{\mathcal{G}}^0 \rangle} = \sum_{n \in \mathbb{N}} a_n a_n^* \langle \Psi_{\lambda_n}, \Psi_{\lambda_n} \rangle + \sum_{m \in \mathbb{N}} a_m^p a_m^{p*} \langle \Psi_{\lambda_m^p}^p, \Psi_{\lambda_m^p}^p \rangle = \sum_{n \in \mathbb{N}} a_n a_n^* + \sum_{m \in \mathbb{N}} a_m^p a_m^{p*}. \quad (43)$$

The wave kinetic energy is given by

$$\begin{aligned} \frac{1}{2} \langle \nabla \mathbf{P}_G^0, \nabla \mathbf{P}_G^0 \rangle &= \frac{1}{2} \sum_{n, n' \in \mathbb{N}} \overline{(a_n e^{i\lambda_n t} + a_n^{p*} e^{-i\lambda_n t})} (a_n e^{i\lambda_n t} + a_n^{p*} e^{-i\lambda_n t}) \langle \nabla \Psi_{\lambda_n}, \nabla \Psi_{\lambda_{n'}} \rangle \\ &+ \frac{1}{2} \sum_{n, m \in \mathbb{N}} \overline{(a_n e^{i\lambda_n t} + a_n^{p*} e^{-i\lambda_n t})} (a_m^p e^{i\lambda_m t} + a_m^{p*} e^{-i\lambda_m t}) \langle \nabla \Psi_{\lambda_n}, \nabla \Psi_{\lambda_m}^p \rangle \\ &+ \frac{1}{2} \sum_{m, m' \in \mathbb{N}} \overline{(a_m^p e^{i\lambda_m t} + a_m^{p*} e^{-i\lambda_m t})} (a_{m'}^p e^{i\lambda_{m'} t} + a_{m'}^{p*} e^{-i\lambda_{m'} t}) \langle \nabla \Psi_{\lambda_m}^p, \nabla \Psi_{\lambda_{m'}}^p \rangle, \end{aligned} \quad (44)$$

where notation

$$\langle \nabla \Psi_{\lambda}, \nabla \Psi_{\lambda'} \rangle = \sum_{e_k \in \mathcal{E}} \int_0^{\ell_{e_k}} \frac{d\Psi_k^\lambda}{dx} \frac{d\Psi_k^{\lambda'}}{dx} dx, \quad (45)$$

has been introduced. It is interesting to mention that each energy mode contribution of (45) is independent of the edge's orientation since it is left invariant from $x \rightarrow -x$ transformation within any edge. From a simple computation, temporal average zeros the cross terms so that (44) reduces to self-energy terms

$$\begin{aligned} \frac{1}{2} \langle \nabla \mathbf{P}_G^0, \nabla \mathbf{P}_G^0 \rangle &= \sum_{n \in \mathbb{N}} a_n a_n^* \langle \nabla \Psi_{\lambda_n}, \nabla \Psi_{\lambda_n} \rangle \\ &+ \sum_{m \in \mathbb{N}} a_m^p a_m^{p*} \langle \nabla \Psi_{\lambda_m}^p, \nabla \Psi_{\lambda_m}^p \rangle. \end{aligned} \quad (46)$$

From integrating by part (45) one finds

$$\begin{aligned} \langle \nabla \Psi_{\lambda}, \nabla \Psi_{\lambda} \rangle &= \sum_{e_k \in \mathcal{E}} \left(\left[\Psi_k^\lambda \frac{d\Psi_k^\lambda}{dx} \right] - \int_0^{\ell_{e_k}} \Psi_k^\lambda \frac{d^2 \Psi_k^\lambda}{dx^2} dx \right) \\ &= \sum_{e_k \in \mathcal{E}} \left[\Psi_k^\lambda \frac{d\Psi_k^\lambda}{dx} \right] + \lambda^2 \langle \Psi_{\lambda}, \Psi_{\lambda} \rangle, \end{aligned} \quad (47)$$

where notation $[]$ is the usual evaluation difference at the frontier of each segment e_k , i.e., at each vertex. In the case where Ψ_{λ} is an eigenfunctions of Δ_G , since the boundary conditions at each vertex are either natural or Dirichlet, this term cancels out. The same applies at almost every vertex for eigenfunctions of Δ_G^p except at the origin vertex x_O where the sum of derivatives is not zero from (28) so that a contribution arises there. Hence,

$$\langle \nabla \Psi_{\lambda_n}, \nabla \Psi_{\lambda_n} \rangle = \lambda_n^2 \langle \Psi_{\lambda_n}, \Psi_{\lambda_n} \rangle = \lambda_n^2, \quad (48)$$

$$\langle \nabla \Psi_{\lambda_m}^p, \nabla \Psi_{\lambda_m}^p \rangle = h_m \Psi_{\lambda_m}^p(x_O)^2 + \lambda_m^{p2}, \quad (49)$$

so that summing (43) and (46) using (48) and (49) leads to the total wave energy

$$\begin{aligned} &\frac{1}{2} \langle \mathbf{P}_G^0, \mathbf{P}_G^0 \rangle + \frac{1}{2} \langle \nabla \mathbf{P}_G^0, \nabla \mathbf{P}_G^0 \rangle \\ &= \sum_{n \in \mathbb{N}} a_n a_n^* (\lambda_n^2 + 1) \\ &+ \sum_{m \in \mathbb{N}} a_m^p a_m^{p*} (h_m \Psi_{\lambda_m}^p(x_O)^2 + \lambda_m^{p2} + 1). \end{aligned} \quad (50)$$

Hence, the total energy of the wave is split into two contributions. First, an imposed external term, the second term of (50)'s right-hand side, composed of amplitude a_n^p deduced from the Fourier decomposition of the trigger, the local amplitude $\Psi_{\lambda_m}^p(x_O)^2$ of the mode at the trigger origin x_O , the eigenvalue λ_m^p of the corresponding excited mode, and the h_m constant for which the secularity condition is met for this eigenvalue. Second, an internal term given by the product between the mode amplitude a_n and the square of its real eigenvalue λ_n . From this, one realizes that this second term [first term of (50)'s right-hand side] is the only transferred energy from the external trigger into the internal modes, feeding the metric-graph cavity internal vibration. This opens a second natural question: under which condition can some extremal amount of energy can be transferred from external to internal waves?

B. Optimal energy transfer conditions

Denoting E^I the transferred energy into internal metric graph natural modes, i.e.,

$$E^I = \sum_{n \in \mathbb{N}} E_n^I = \sum_{n \in \mathbb{N}} a_n a_n^* (\lambda_n^2 + 1). \quad (51)$$

Defining the vector $\mathbf{\Pi}^n = \mathbf{\Pi}^{nT} \cdot \hat{\mathbf{n}}$ from the product of matrix $\mathbf{\Pi}^{nT}$, being the transposed of $\mathbf{\Pi}^n$, with unit-vector $\hat{\mathbf{n}}$ whose components $\mathbf{n}_i = \delta_{in}$, from (41) each component a_n reads $a_n = -\mathbf{\Pi}^n \cdot \mathbf{a}^p$ so that, using the fact that both vector \mathbf{a} and \mathbf{a}^p are purely imaginary from (34) and (41) the energy reads

$$E^I = \sum_{n \in \mathbb{N}} E_n^I = - \sum_{n \in \mathbb{N}} (\mathbf{\Pi}^n \cdot \mathbf{a}^p)^2 (\lambda_n^2 + 1). \quad (52)$$

Since the derivative of (52) with respect to any component of vector \mathbf{a}^p is proportional to $(\mathbf{\Pi}^n \cdot \mathbf{a}^p)$, it is zero for the trivial condition $\mathbf{a}^p = 0$ for which a minimum energy is achieved. A maximal condition can nevertheless be found from considering a constraint over finite possible values of vector \mathbf{a}^p components. This constraint comes from a prescribed finite energy of the triggering function $P_O(\tau)$ given by its Fourier decomposition from the Parseval-Plancherel equality

$$\int_{\mathbb{R}} P_O^2(\tau) d\tau = \|\mathbf{P}_O\|^2 = \sum_{m \in \mathbb{N}} P_{Om}^2, \quad (53)$$

a maximum energy transfer can be set from defining function

$$J_n(\mathbf{a}^p, \lambda_M) = E_n^I - \lambda_M (\|\mathbf{P}_O\|^2 - E_{P_O}), \quad (54)$$

where the constraint $\|\mathbf{P}_{Om}\|^2 = E_{P_o}$ is set from minimizing J_n over the Lagrangian multiplier λ_M . Minimizing J_n over both \mathbf{a}^p and λ_M leads to

$$\lambda_M = -\frac{\lambda_n^2 + 1}{E_{P_o}} (\boldsymbol{\Pi}^m \cdot \mathbf{a}^p)^2$$

$$(\boldsymbol{\Pi}^m \cdot \mathbf{a}^p) a_m^p = E_{P_o} \frac{\Pi_m^n}{4h_m^2 \Psi_{\lambda_m}^p(x_o)^2}. \quad (55)$$

Using the simple relation between vector \mathbf{a}^p components and \mathbf{P}_O given in (34), and defining the unit vector direction of the triggering Fourier components $\mathbf{p}_O = \mathbf{P}_O / \|\mathbf{P}_O\|$, then (55) simplifies to

$$(\boldsymbol{\Pi}^m \cdot \mathbf{p}_O) \mathbf{p}_O = \boldsymbol{\Pi}^m. \quad (56)$$

The solution of (56) is then simply

$$\mathbf{p}_O = \boldsymbol{\Pi}^m / \|\boldsymbol{\Pi}^m\|. \quad (57)$$

(57) states that the optimal energy transfer is obtained when the triggering Fourier components vector is aligned with vector $\boldsymbol{\Pi}^m$ whatever its amplitude.

V. DAMPED WAVES SOLUTIONS

This section now considers the wave damping with the viscous damping model discussed in Sec. II A. Following Refs. [21,28] the solution for the damped wave pressure problem (1) is searched within a multi-time-scale expansion solution. Using long-time $T = \epsilon\tau$ so that $\partial_t \equiv (\partial_\tau + \epsilon\partial_T)$, a regular approximate solution for the pressure solution over \mathcal{G} (1) is searched as

$$\mathbf{P}_G = \mathbf{P}_G^0 + \epsilon \mathbf{P}_G^1 + \dots \quad (58)$$

Along with the pressure fields the long-time wave amplitude are also decomposed into such multiscale asymptotic

expansion so that for both the homogeneous and particular part, so that for each $n, m \in \mathbb{N}$

$$A_n(T) = A_n^0(T) + \epsilon A_n^1(T) + \dots, \quad (59)$$

$$A_m^p(T) = A_m^{0p}(T) + \epsilon A_m^{1p}(T) + \dots \quad (60)$$

The long-time damping amplitudes $A_n^0(T)$ of the leading-order solution is then found from analyzing the first-order one in Laplace domain from what is called the secularity condition [37]. The Laplace transform of field denoted with tildes, is considered, so that, using (59), (60) the Laplace transform of the leading order (23) reads

$$\tilde{\mathbf{P}}_G^0 = \sum_{n \in \mathbb{N}} \left(\frac{A_n^0(T) a_n^0}{s - i\lambda_n} + cc \right) \boldsymbol{\Psi}_{\lambda_n}$$

$$+ \sum_{m \in \mathbb{N}} \left(\frac{A_m^{0p}(T) a_m^{0p}}{s - i\lambda_m^p} + cc \right) \boldsymbol{\Psi}_{\lambda_m^p}, \quad (61)$$

where coefficients a_n^0 are identical with coefficients a_n computed in Sec. III where the $\epsilon = 0$ limit has been considered. At first order (1) leads within each edge k to

$$\left(\frac{\partial^2}{\partial \tau} - \frac{\partial^2}{\partial x^2} \right) p_k^1 = 2 \left(\frac{\partial \tau_w^0}{\partial x} - \frac{\partial}{\partial T} \frac{\partial}{\partial \tau} p_k^0 \right), \quad (62)$$

where within each edge, the pressure leading order and first order are, respectively, denoted p_k^0 and p_k^1 for $k \in E$. Since, the first-order problem is then decomposed into the Laplacian eigenfunctions

$$\mathbf{P}_G^1 = \sum_{n \in \mathbb{N}} [a_n^1(\tau) + c.c.] \boldsymbol{\Psi}_{\lambda_n} + \sum_{m \in \mathbb{N}} [a_m^{1p}(\tau) + c.c.] \boldsymbol{\Psi}_{\lambda_m^p}. \quad (63)$$

From (61), one can evaluate the right-hand side of (62) in the Laplace domain, which reads, using the Laplace transform of the wall-shear stress (3)

$$2 \left(\frac{\partial \tilde{\tau}_w^0}{\partial x} - \frac{\partial}{\partial T} s \tilde{\mathbf{P}}_G^0 \right) = 2 \left(\sum_{n \in \mathbb{N}} \left[\frac{a_n^0}{s - i\lambda_n} \left(A_n^0 \frac{\sqrt{s}}{s} \lambda_n^2 - s \frac{\partial A_n^0}{\partial T} \right) + cc \right] \boldsymbol{\Psi}_{\lambda_n} + \sum_{m \in \mathbb{N}} \left[\frac{a_m^{0p}}{s - i\lambda_m^p} \left(A_m^{0p} \frac{\sqrt{s}}{s} \lambda_m^{p2} - s \frac{\partial A_m^{0p}}{\partial T} \right) + cc \right] \boldsymbol{\Psi}_{\lambda_m^p} \right). \quad (64)$$

Writing (62) in Laplace domain while using (64), the first-order problem written on \mathcal{G} reads

$$(s^2 - \Delta_G) \mathbf{P}_G^1 = 2 \left(\sum_{n \in \mathbb{N}} \left[\frac{a_n^0}{s - i\lambda_n} \left(A_n^0 \frac{\sqrt{s}}{s} \lambda_n^2 - s \frac{\partial A_n^0}{\partial T} \right) + c.c. \right] \boldsymbol{\Psi}_{\lambda_n} + \sum_{m \in \mathbb{N}} \left[\frac{a_m^{0p}}{s - i\lambda_m^p} \left(A_m^{0p} \frac{\sqrt{s}}{s} \lambda_m^{p2} - s \frac{\partial A_m^{0p}}{\partial T} \right) + c.c. \right] \boldsymbol{\Psi}_{\lambda_m^p} \right). \quad (65)$$

Projecting (65) over $\boldsymbol{\Psi}_{\lambda_n}$ leads to

$$\frac{1}{2} [\tilde{a}_n^1 + c.c.] + \sum_{m \in \mathbb{N}} [\tilde{a}_m^{1p}(s) + c.c.] \frac{s^2 + \lambda_m^{p2}}{s^2 + \lambda_n^2} \boldsymbol{\Pi}_{nm}$$

$$= \left[\frac{a_n}{(s - i\lambda_n)^2} \left(\frac{A_n \sqrt{s}}{s} \lambda_n^2 - s \frac{\partial A_n}{\partial T} \right) + c.c. \right] + \sum_{m \in \mathbb{N}} \left(\left[\frac{a_m^p}{(s - i\lambda_m^p)} \left(\frac{A_m^p \sqrt{s}}{s} \lambda_m^{p2} - s \frac{\partial A_m^p}{\partial T} \right) + c.c. \right] \right) \boldsymbol{\Pi}_{nm}. \quad (66)$$

Furthermore, projecting (65) over $\Psi_{\lambda_n^p}$ leads to

$$\begin{aligned} & \sum_{m' \in \mathbb{N}} \mathbf{\Pi}_{mm'}^{pp} \frac{[\tilde{a}_{m'}^{1p} + \text{c.c.}]}{2} + \sum_{n \in \mathbb{N}} \frac{[\tilde{a}_n^1(s) + \text{c.c.}]}{2} \frac{s^2 + \lambda_n^2}{s^2 + \lambda_m^2} \mathbf{\Pi}_{nm} \\ &= \left[\frac{a_m^p}{(s - i\lambda_m^p)^2} \left(\frac{A_m^p \frac{\sqrt{s}}{s} \lambda_m^{2p} - s \frac{\partial A_m^p}{\partial T}}{(s + i\lambda_m^p)} \right) + \text{c.c.} \right] + \sum_{m' \neq m} \left(\frac{a_{m'}^p}{(s^2 + \lambda_m^{p2})(s - i\lambda_{m'}^p)} \left(\frac{A_{m'}^p \frac{\sqrt{s}}{s} \lambda_{m'}^{p2} - s \frac{\partial A_{m'}^p}{\partial T}}{(s + i\lambda_{m'}^p)} \right) + \text{c.c.} \right) \mathbf{\Pi}_{mm'}^{pp} \\ &+ \sum_{n \in \mathbb{N}} \left(\left[\left(\frac{a_n}{s - i\lambda_n} \right) \left(\frac{A_n \frac{\sqrt{s}}{s} \lambda_n^2 - s \frac{\partial A_n}{\partial T}}{s^2 + \lambda_m^2} \right) + \text{c.c.} \right] \right) \mathbf{\Pi}_{nm}. \end{aligned} \quad (67)$$

It is now crucial to note that only the first line of (66) and (67)'s right-hand side have double poles, respectively, at $s = \pm i\lambda_n$ for (66) and $s = \pm i\lambda_m^p$ for (67), whereas both second lines of (66) and second and third lines of (67)'s right-hand side display only simple poles. Only double poles in Laplace domain lead to time-diverging terms: these are called resonant poles [21,28]. These double poles are associated with resonance conditions between the (65)'s right-hand side and the natural frequencies of the (65)'s left-hand side. These resonance conditions produce a linear divergence term upon the fast time τ of \tilde{a}_n^1 and \tilde{a}_m^{p1} as can be seen from the inverse Laplace transform of the double poles through Cauchy's residue theorem

$$\mathcal{L}^{-1} \left(\frac{1}{(s \pm i\lambda_n)^2} \right) (\tau) = \lim_{s \rightarrow \pm i\lambda_n} (\partial_s e^{s\tau}) = \tau e^{\pm i\lambda_n \tau}. \quad (68)$$

It is interesting to note that the second line of (66) and the second and third lines of (67) do not have double poles but only simple ones because the eigenvalues of the operator Δ_G can not have resonance with those of Δ_G^p . The secularity condition is built to remove those divergent terms, i.e., double poles, so that both first lines of (66) and (67) have to cancel. Imposing this secularity condition for the first line of (66) leads to

$$\begin{aligned} \lim_{s \rightarrow i\lambda_n} \left(A_n \frac{\sqrt{s}}{s} \lambda_n^2 - s \frac{\partial A_n}{\partial T} \right) &= 0, \\ \lim_{s \rightarrow -i\lambda_n} \left(A_n^* \frac{\sqrt{s}}{s} \lambda_n^2 - s \frac{\partial A_n^*}{\partial T} \right) &= 0, \end{aligned} \quad (69)$$

leading to the same consistent secularity solution

$$A_n(T) = e^{-\sqrt{-i\lambda_n}T} = e^{-\left(\frac{1-i}{\sqrt{2}}\right)\sqrt{\lambda_n}T}, \quad (70)$$

using the normalization condition (25). A very similar result is obtained canceling the double pole of the first line of (67)'s right-hand side

$$\begin{aligned} \lim_{s \rightarrow i\lambda_m^p} \left(A_m^p \frac{\sqrt{s}}{s} \lambda_m^{p2} - s \frac{\partial A_m^p}{\partial T} \right) &= 0, \\ \lim_{s \rightarrow -i\lambda_m^p} \left(A_m^{p*} \frac{\sqrt{s}}{s} \lambda_m^{p2} - s \frac{\partial A_m^{p*}}{\partial T} \right) &= 0, \end{aligned} \quad (71)$$

leading to a parallel damping of the particular solution using normalization (31)

$$A_m^p(T) = e^{-\sqrt{-i\lambda_m^p}T} = e^{-\left(\frac{1-i}{\sqrt{2}}\right)\sqrt{\lambda_m^p}T}. \quad (72)$$

Now, using (70) and (72) in (23) leads to the damped leading-order solution

$$\begin{aligned} \mathbf{P}_G^0 &= \sum_{n \in \mathbb{N}} e^{-\sqrt{\frac{\lambda_n}{2}}T} (a_n^0 e^{i\sqrt{\frac{\lambda_n}{2}}T} e^{i\lambda_n t} + \text{c.c.}) \Psi_{\lambda_n} \\ &+ \sum_{m \in \mathbb{N}} e^{-\sqrt{\frac{\lambda_m^p}{2}}T} (a_m^{p0} e^{i\sqrt{\frac{\lambda_m^p}{2}}T} e^{i\lambda_m^p t} + \text{c.c.}) \Psi_{\lambda_m^p}. \end{aligned} \quad (73)$$

VI. ILLUSTRATION WITH AN EXAMPLE

In this section we illustrate the previous solution over a very simple three-star graph illustrated in Fig. 1 having noncommensurable length with the considered modes, i.e., $\ell_{ij}\lambda_n \neq n\pi$ and $\ell_{ij}\lambda_m^p = \ell_{ij}m\pi/T_e \neq m\pi$. The adjacency matrix of the three-star graph of Fig. 1 reads

$$\mathbf{A} = \begin{bmatrix} 0 & 1 & 0 & 0 \\ 1 & 0 & 1 & 1 \\ 0 & 1 & 0 & 0 \\ 0 & 1 & 0 & 0 \end{bmatrix}. \quad (74)$$

Using definition (10) the secular matrix reads

$$\mathfrak{A}(\lambda, \mathbf{h}) = \begin{bmatrix} -\cot(\ell_{21}\lambda) & \frac{1}{\sin(\ell_{21}\lambda)} & 0 & 0 \\ \frac{1}{\sin(\ell_{21}\lambda)} & -\frac{h_m}{\lambda} - \cot(\ell_{21}\lambda) - \cot(\ell_{32}\lambda) - \cot(\ell_{24}\lambda) & \frac{1}{\sin(\ell_{32}\lambda)} & \frac{1}{\sin(\ell_{24}\lambda)} \\ 0 & \frac{1}{\sin(\ell_{32}\lambda)} & -\cot(\ell_{32}\lambda) & 0 \\ 0 & \frac{1}{\sin(\ell_{24}\lambda)} & 0 & -\cot(\ell_{24}\lambda) \end{bmatrix}, \quad (75)$$

whose determinant is

$$\det \mathfrak{A}(\lambda, \mathbf{h}) = \left[\left[\frac{h_m}{\lambda} \cot(\ell_{24}\lambda) - 1 \right] \cot(\ell_{23}\lambda) - \cot(\ell_{24}\lambda) \right] \cot(\ell_{21}\lambda) - \cot(\ell_{23}\lambda) \cot(\ell_{24}\lambda). \quad (76)$$

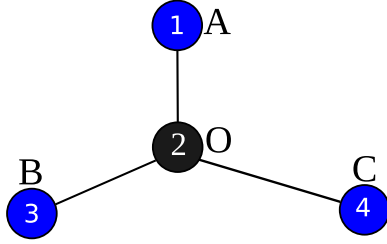
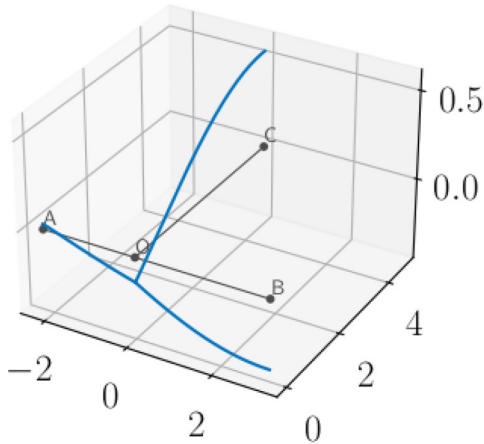
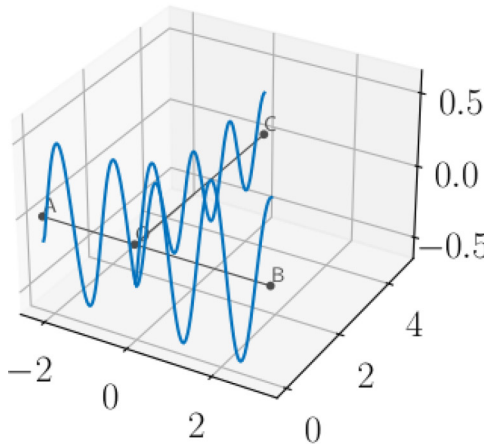


FIG. 1. Three-star metric graph having length $\ell_{21} = 2.211$, $\ell_{23} = 3.111$, and $\ell_{24} = 4.711$ where the triggering is applied at origin point O , i.e., at vertex #2.

Numerically solving for $\det \mathfrak{A}(\lambda_n, \mathbf{0}) = 0$ gives the eigenvalues λ_n of the Kirchhoff modes. This spectrum is complemented with the vertex vector ϕ_{λ_n} of quantum graph modes n (8) obtained from computing the one-dimensional null space of matrix $\mathfrak{A}(\lambda_n, \mathbf{0})$ (here a four-vector), which then sets Ψ_{λ_n} . Table I provides the λ_n and ϕ_{λ_n} values of the first 20 Kirchhoff modes. Figure 2 illustrates the first two Kirchhoff modes Ψ_{λ_1} and Ψ_{λ_2} , showing as expected an increasing number of minima and maxima as λ_n increases.

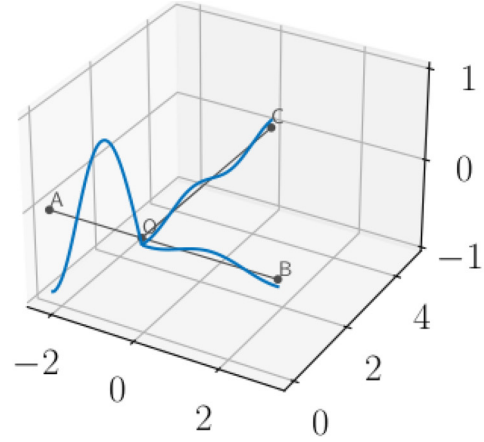


(a) Kirchhoff mode Ψ_{λ_1} .

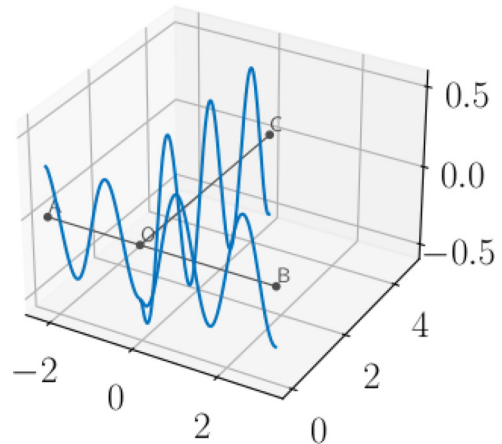


(b) Kirchhoff mode Ψ_{λ_2} .

FIG. 2. First two Kirchhoff eigenmode of the three-star graph 1.



(a) Kirchhoff-Robin-Fourier $\Psi_{\lambda_1^p}$.



(b) Kirchhoff-Robin-Fourier $\Psi_{\lambda_2^p}$.

FIG. 3. First two Kirchhoff-Robin-Fourier eigenmodes of the three-star graph 1.

Furthermore, imposing the Fourier modes $\lambda_m^p = m\pi/T_e$ and solving for h_m such that $\det \mathfrak{A}(\lambda_m^p, \mathbf{h} = h_m \hat{\mathbf{e}}^0) = 0$, with vector $\hat{\mathbf{e}}^0$ being the unit vector on vertex $v_O = 2$, permits to find $\phi_{\lambda_m^p}$ from the null space of $\mathfrak{A}(\lambda_m^p, \mathbf{h} = h_m \hat{\mathbf{e}}^0)$, which then provides the Kirchhoff-Robin-Fourier modes $\Psi_{\lambda_m^p}$. Table II provides the h_m values, as well as the λ_m^p and $\phi_{\lambda_m^p}$ of the first 20 Kirchhoff-Robin-Fourier modes. Figure 3 also illustrates the first two Kirchhoff-Robin-Fourier modes $\Psi_{\lambda_1^p}$ and $\Psi_{\lambda_2^p}$ (using the graphs structure of the PYTHON's GRAFIDI library [38] nested with NETWORKX's one [39]). A pulsed, Gaussian closure law

$$P_O(t) = e^{-\frac{(t-t_0)^2}{2\tau_e^2}}, \tag{77}$$

is chosen with $t_0 = 1$ and $\tau_e = 0.1$. This pulsed law is almost zero at $t = 0$ and $t = T_e$ (chosen as $T_e = 4.75$ in Fig. 4) so that the condition for Fourier series decomposition over a finite-time interval is met. One can see in Fig. 4 an example of full solution computed without and with damping correction. As can be seen, since the closure law is localized in time, it excites a rather larger number of Fourier modes, resulting in a spatially oscillating solution.

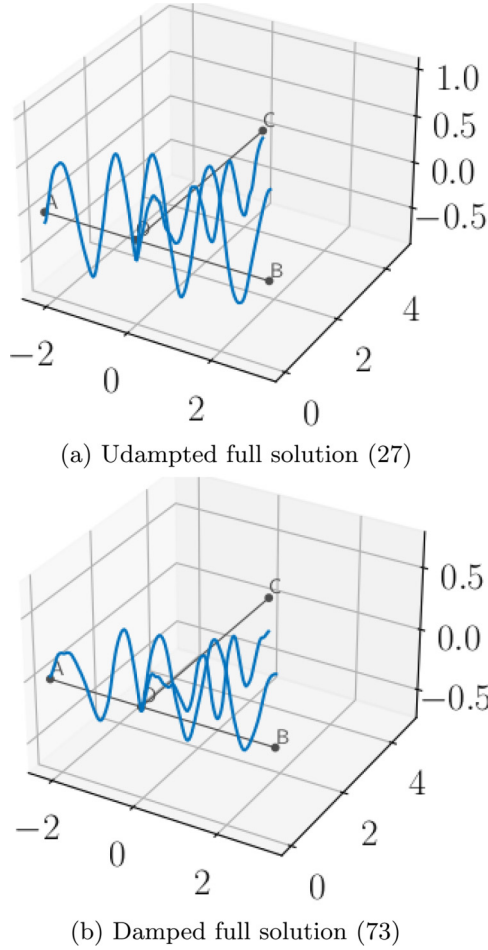


FIG. 4. Comparison between undamped and damped solution at $t = 3$ for closure law (77) taken for $t_0 = 1$, $\tau_e = 0.1$, $T_e = 4.75$.

VII. DISCUSSION

This paper has addressed how a finite-time excitation happening within a specific location (called the origin) of the network propagates into it as a wave train. This propagating wave train is decomposed into the stationary waves modes of the metric graph, as classically done in simple cavities. However, since a graph has a complex topology (provided by its adjacency matrix), the stationary modes of vibrations given by the quantum-graph eigenfunction of the Laplacian operator are also complex. However, these quantum-graph modes provide the (infinite-dimensional) discrete base for propagating wave decomposition, as the canonical decomposition of the harmonic oscillator in quantum mechanics. In the absence of damping mechanism, Sec. III shows how the undamped propagating wave decomposes into two distinct parts: (i) a specific one, leading to the particular part of the stationary-wave decomposition, having its own spectrum of vibration λ_m^p chosen as Fourier modes and eigenfunctions depending on the excitation origin \mathbf{x}_O and (ii) the natural vibration modes given by the metric graph's Laplacian eigenfunction, associated with their specific homogeneous spectrum of vibration λ_n . Section III found how the amplitude of the particular part can be deduced from the Fourier-mode decomposition of the finite-time excitation. Furthermore, projection matrix $\mathbf{\Pi}'$ permits us to

deduce the natural homogeneous modes amplitude from the particular ones. We present explicit quasianalytical solutions for the wave train. These solutions have then permitted us to address several interesting issues.

First, provided that the origin and the finite-time excitation can be changed, it is interesting to find the optimal excitation able to feed the natural cavity modes, i.e., to produce optimal energy into the natural cavity modes. This question arises since the excitation naturally decomposes into the particular modes, which secondarily transmit their energy to natural modes. Section IV A derives the total energy of the wave inside a metric graph, showing that only the internal part, denoted E^I , is able to feed natural cavity vibrations modes. Looking for optimal conditions for energy transfer between the excitation's Fourier-mode decomposition and the natural cavity mode, Sec. IV B shows that an optimal energy transfer into the n th natural mode is achieved when the Fourier mode decomposition vector of the triggering \mathbf{P}_O is colinear with vector $\mathbf{\Pi}^n = \mathbf{\Pi}'^T \cdot \hat{\mathbf{n}}$. This simple geometrical result permits us to consider a mode-to-mode specific triggering, but it is important to stress that this energy transfer can be shaped optimally for a single natural mode only. Also, it is worth mentioning that even if this optimal condition is general for any origin location, it differs for each chosen origin since matrix $\mathbf{\Pi}'$ depends on the chosen origin \mathbf{x}_O for the finite-time excitation.

It is also interesting to note that the lowest natural energy modes $n = 1$, having eigenvalue λ_1 and waveform Ψ_{λ_1} , a sort of ground state of natural vibrations, could be a natural choice for such optimal harvesting of external triggers. This choice could be justified from the fact that this mode is the less damped one, as now discussed.

Second, analyzing the acoustic damping established in fluid mechanics for the boundary-layer diffusion of axial momentum transfer, Sec. V derives a multi-time-scale expansion analysis associated fast time-scale τ and long time-scale T of the wave propagation. This asymptotic framework applied within quantum-graph waveform decomposition, leads to an explicit analytical result for the leading-order wave propagation damping. This leading-order damping is surprisingly simple, since each mode is exponentially damped over long time-scale T , with a damping rate directly related to their eigenvalue λ_n and λ_m^p , i.e., proportional to $\sqrt{\lambda_n/2}$ and $\sqrt{\lambda_m^p/2}$. This result shows that the higher the energy mode, the higher damping rate. This general theoretical result established within a secularity condition of resonant modes provides a significant long time-scale $\sqrt{2}/(\sqrt{\lambda_2} - \sqrt{\lambda_1})$ for which all $n > 1$ modes are damped but for the remaining cavity natural ground-state vibration $n = 1$. Similarly $\sqrt{2}/(\sqrt{\lambda_2^p} - \sqrt{\lambda_1^p})$ gives the time scale for the particular solution ground state to survive over highest-order modes $m > 1$. Here again these theoretical results have been established within a general context and apply to any metric graph. They surprisingly generalize the result obtained within a single pipe [21]. They furthermore give supplementary physical insights for each mode eigenvalue. Since the wave energy of each mode E_n^I is proportional to its amplitude, i.e., $E_n^I = A_n A_n^* a_n a_n^* (\lambda_n^2 + 1)$, it is thus exponentially decaying for damped wave so that $E_n^I \sim e^{-\sqrt{2\lambda_n}T}$. Hence, not only each mode eigenvalue sets

the corresponding vibration mode energy level but also its damping rate. This conclusion is obviously specific to the considered hydrodynamic damping model.

Nevertheless, it is known in other area that weak nonlinearities are responsible for wave damping, whereby a small parameter can be considered, e.g., spin-wave propagation [22]. Hence, the generic perturbed multiscale approach proposed in this study might be adapted to other contexts.

VIII. CONCLUSION

This paper considers a one-dimensional model of wave propagation inside a metric graph, i.e., a long wavelength approximation propagation within a network of wirelike connections, triggered by an external event arising at one vertex origin. Even though a general case of (compact and not-multigraph) graph has been considered a number of analytical results have been established.

It has been found that the external trigger induces two families of secondary waves into the network: (i) an external one specific to the origin location (ii) an internal one provided by the natural modes of the metric graph. Canonical decomposition of the wave modes has been set up, the amplitude of which have been found explicitly for any finite-time triggering shape. Furthermore, an explicit condition on the finite-time trigger shape has been found, given its origin, in order to obtain an optimal energy transfer into one single internal mode.

Finally, this paper has analyzed the influence of boundary-layer dissipation on the wave propagation within the network. Within an established damping model for which the wall-shear rate is a time convolution of the pressure gradient with a diffusion kernel, a multi-time-scale analysis of the wave dynamics has been performed. This analysis has permitted us to establish the damping rate of each mode from the secularity condition of resonant modes. The obtained final result is surprisingly simple and general: the damping rate of each mode is exponential with a corresponding time decay directly related to the mode's eigenvalue. This results holds for any metric graph and any triggering event origin and shape. Knowing the decaying rates of propagating modes inside the network is a precious information that might benefit further investigations in various physical domains.

APPENDIX

Three movies are proposed in the Supplemental Material (SM) [40] to illustrate the quantum-graph wave within a

three-star metric graph, with (i.e., for water-hammer small parameter $\epsilon = 0.1, 0.01$) and without damping.

1. Shear rate derivation

This Appendix considers the boundary layer structure of an acoustic wave propagating into a straight pipe along its main axis (which is the metric graph's edge). Whatever the transverse shape of the pipe, this boundary layer is a thin layer described by a rescaled variable y ($y = 0$ at the pipe's wall whereas matching conditions have to be met has $y \gg 1$). Within this layer, even if the fluid pressure does not depend on y and is the same as in the core of the pipe, this is not the case for the perturbed longitudinal velocity traveling with the wavefront. Albeit the wavefront velocity has a plane-wave structure not varying in the transverse direction, in the layer the velocity varies, because it has to match a no-slip condition at the pipe's wall. Following Refs. [21,28] the dimensionless boundary-layer problem associated with the longitudinal velocity $w(y, t)$ perturbation within boundary-layer thickness is:

$$\left(\frac{\partial}{\partial t} - \frac{\partial^2}{\partial y^2} \right) w = -\frac{\partial}{\partial z} p. \quad (\text{A1})$$

(A1) is a diffusion problem driven by the longitudinal pressure gradient associated with no-slip boundary condition

$$w(y, t)|_{y=0} = 0. \quad (\text{A2})$$

The Laplace transform of (A1) reads

$$\left(s - \frac{\partial^2}{\partial y^2} \right) \tilde{w} = -\frac{\partial}{\partial z} \tilde{p}. \quad (\text{A3})$$

The solution for \tilde{w} with boundary condition (A2) is

$$\tilde{w} = -\frac{1}{s} (1 - e^{-\sqrt{s}y}) \frac{\partial}{\partial z} \tilde{p}. \quad (\text{A4})$$

From (A4), one can evaluate the shear rate

$$\frac{\partial \tilde{w}}{\partial y} = -\frac{\sqrt{s}}{s} e^{-\sqrt{s}y} \frac{\partial}{\partial z} \tilde{p}, \quad (\text{A5})$$

which, evaluated at $y = 0$ gives the wall-shear stress

$$\tilde{\tau}_w = \frac{\partial \tilde{w}}{\partial y} \Big|_{y=0} = -\frac{\sqrt{s}}{s} \frac{\partial}{\partial z} \tilde{p}. \quad (\text{A6})$$

2. Numerical evaluation of eigenmodes on the three-star example

TABLE I. First 20 Kirchhoff eigenmodes for the three-star graph illustrated in Fig. 1 having $\ell_{21} = 2.211$, $\ell_{23} = 3.111$, and $\ell_{24} = 4.711$.

n	λ_n	μ_n	ϕ_1	ϕ_2	ϕ_3	ϕ_4
1	0.3881987759	0.721871103	-0.2964486625	-0.1937941785	-0.5456176736	0.7595152146
2	4.7117467165	0.870663106	0.5961287943	-0.3256461334	0.6541514685	0.3326723804
3	6.3525865114	0.747238735	0.6621539408	0.0605673071	0.0991111588	0.7403112441
4	12.4788910454	0.807255566	0.3962512926	-0.3072388027	-0.7091748792	0.4956412231
5	15.6637713517	0.715622334	0.0250483717	-0.0249778073	-0.7076024501	0.7057247770
6	18.8328225632	0.828397911	-0.4571083665	0.3189075512	-0.7049346172	0.4386537365
7	21.8647164683	0.877339202	-0.7303136021	0.2516560345	0.5482473241	-0.3205248111
8	24.9689545929	0.740647579	-0.6023871790	-0.1364432674	0.2094689958	0.7580472684
9	28.1697479121	0.834695986	0.5045162370	0.4304968982	0.4548185059	0.5943701826
10	28.5032976758	0.817198780	-0.4200833880	-0.4126076818	-0.5436874373	0.5980709143
11	37.6697929771	0.713414664	0.2875184547	0.1521514201	-0.5394990582	0.7766104878
12	39.0342472648	0.767642573	-0.7240653074	0.0258486717	-0.0445497912	0.6878056360
13	40.9700198335	0.788614889	0.7589439659	-0.0675152885	0.1450308764	0.6311986909
14	46.9910214079	0.718634694	0.1655504268	-0.1435465042	0.6484171240	0.7290697433
15	47.6534209076	0.719792691	-0.0764957925	0.0745746258	-0.7114791028	0.6945390596
16	50.3790954261	0.774936991	-0.7289459417	-0.0860765421	0.1039341549	0.6711380889
17	53.5507183138	0.771439486	-0.7173461300	0.0989350844	0.1053306351	0.6815657241
18	56.6752993239	0.822768128	-0.6273590268	-0.3495142650	0.3509945675	-0.6008853831
19	59.8244568982	0.890364225	-0.5139237713	-0.4819467842	-0.5205770943	0.4822957012
20	63.0481713312	0.799147437	0.4084803861	0.3870989844	-0.5340092449	0.6309772395

TABLE II. First 20 Kirchhoff-Robin-Fourier eigenmodes for the three-star graph illustrated in Fig. 1 having $\ell_{21} = 2.211$, $\ell_{23} = 3.111$ and $\ell_{24} = 4.711$ and $T_e = 3$.

m	h_m	λ_m^p	μ_m^p	ϕ_1^p	ϕ_2^p	ϕ_3^p	ϕ_4^p
1	0	0	0.390892211472686	-1/2	-1/2	-1/2	-1/2
2	-5.6761067886	1.0471975512	0.866025403795264	0.9892583868	-0.0807141968	-0.0829455557	0.0892922023
3	27.0707525154	2.0943951024	0.9401125299521663	0.4221005562	-0.4164806859	-0.4659447130	-0.6567118722
4	-0.4290295559	3.1415926536	0.7948670679344159	0.6805666312	0.1651049412	0.2154030627	-0.6805666312
5	6.5175845447	4.1887902048	0.768237183460571	-0.1894893283	-0.1794650216	-0.3001564240	0.9174923551
6	-7.1650559575	5.2359877560	0.6812082204984988	0.6200042387	-0.2462333756	-0.6200042387	-0.4129874246
7	55.5162277169	6.2831853072	0.8350356746495707	-0.1883438974	0.1661741682	0.9944415719	-0.1883438974
8	11.5804687872	7.3303828584	0.8084598283517545	0.1035548983	0.0560357562	-0.9914580544	0.0561008333
9	-33.6097040206	8.3775804096	0.8041075875409945	0.3141919519	0.2494653931	-0.8752580122	-0.2701367193
10	-0.7590488822	9.4247779608	0.8259789365448891	-0.4843748682	0.3248632377	-0.6520934373	0.4843748682
11	34.2980882012	10.4719755120	0.8234497892328267	0.3518424919	-0.2408527596	0.3518424919	0.8333088683
12	55.6965505609	11.5191730632	0.7130645733724921	-0.1814287152	-0.1419481596	0.1701856250	0.9581081329
13	57.2817539194	12.5663706144	0.6680245542586459	-0.6129066270	-0.3413127558	0.3635884154	-0.6129066270
14	224.8175097958	13.6135681656	0.8170393561807747	0.5292125785	-0.4621414754	0.4654542977	0.5382486415
15	-236.9056511100	14.6607657168	0.8676319218284292	-0.8113900188	0.3362202104	-0.3383820281	0.3377866347
16	-177.2636641898	15.7079632679	0.9243109267767916	0.5073295340	0.4773366021	-0.5073295340	-0.5073295340
17	-62.2157763947	16.7551608191	0.8787224758462283	-0.8764906890	-0.2286251516	0.2729761162	-0.3240040928
18	-261.5751276361	17.8023583703	0.9087615809939374	0.2813551634	-0.2766973864	0.4015263996	0.8264710393
19	8.8862900582	18.8495559215	0.7158240806023455	-0.6984669677	0.0700993426	-0.1391900580	-0.6984669677
20	-37.9008804040	19.8967534727	0.7630641138224415	-0.2386874075	-0.2386450053	0.8199840174	-0.4622803198

[1] L. Pauling, The diamagnetic anisotropy of aromatic molecules., *J. Chem. Phys.* **4**, 673 (1936).
 [2] T. Kottos and U. Smilansky, Periodic orbit theory and spectral statistics for quantum graphs, *Ann. Phys. (NY)* **274**, 76 (1999).

[3] J.-P. Roth, Le spectre du laplacien sur un graphe, in *Colloque de Théorie du Potentiel* (Springer, Berlin, 1983), pp. 521–539.
 [4] S. Yalouz, V. Pouthier, and C. Falvo, Exciton-phonon dynamics on complex networks: Comparison between a perturbative

- approach and exact calculations, *Phys. Rev. E* **96**, 022304 (2017).
- [5] T. Kottos and U. Smilansky, Quantum chaos on graphs, *Phys. Rev. Lett.* **79**, 4794 (1997).
- [6] Y. Dabaghian, Periodic orbit theory and the statistical analysis of scaling quantum graph spectra, *Phys. Rev. E* **75**, 056214 (2007).
- [7] U. Smilansky, Delay-time distribution in the scattering of time-narrow wave packets. (i), *J. Phys. A: Math. Theor.* **50**, 215301 (2017).
- [8] U. Smilansky and H. Schanz, Delay-time distribution in the scattering of time-narrow wave packets (ii)-quantum graphs, *J. Phys. A: Math. Theor.* **51**, 075302 (2018).
- [9] S. Gnuzmann and D. Waltner, Stationary waves on nonlinear quantum graphs: General framework and canonical perturbation theory, *Phys. Rev. E* **93**, 032204 (2016).
- [10] A. V. Azotsev and N. A. Pertsev, Excitation of high-frequency magnon modes in magnetoelastic films by short strain pulses, *Phys. Rev. Mat.* **4**, 064418 (2020).
- [11] B. Z. Rameshti, S. V. Kusminskiy, J. A. Haigh, K. Usami, D. Lachance-Quirion, Y. Nakamura, C.-M. Hu, H. X. Tang, G. E. W. Bauer, and Y. M. Blanter, Cavity magnonics, *Phys. Rep.* **979**, 1 (2022).
- [12] A. V. Sekretenko, S. S. Gavrilov, and V. D. Kulakovskii, Polariton-polariton interactions in microcavities under a resonant 10 to 100 picosecond pulse excitation, *Phys. Rev. B* **88**, 195302 (2013).
- [13] M. Białous, V. Yunko, S. Bauch, M. Ławniczak, B. Dietz, and L. Sirko, Power spectrum analysis and missing level statistics of microwave graphs with violated time reversal invariance, *Phys. Rev. Lett.* **117**, 144101 (2016).
- [14] V. Yunko, M. Białous, and L. Sirko, Edge switch transformation in microwave networks, *Phys. Rev. E* **102**, 012210 (2020).
- [15] A. Rehemangiang, M. Richter, U. Kuhl, and H. J. Stoeckmann, Spectra and spectral correlations of microwave graphs with symplectic symmetry, *Phys. Rev. E* **97**, 022204 (2018).
- [16] T. Hofmann, J. Lu, U. Kuhl, and H.-J. Stoeckmann, Spectral duality in graphs and microwave networks, *Phys. Rev. E* **104**, 045211 (2021).
- [17] W. Zhang, X. Zhang, J. Che, J. Lu, M. Miski-Oglu, and B. Dietz, Experimental study of closed and open microwave waveguide graphs with preserved and partially violated time-reversal invariance, *Phys. Rev. E* **106**, 044209 (2022).
- [18] M. Gaio, D. Saxena, J. Bertolotti, D. Pisignano, A. Camposeo, and R. Sapienza, A nanophotonic laser on a graph, *Nature Commun.* **10**, 226 (2019).
- [19] S. Ma, T. M. Antonsen, and S. M. Anlage, Eigenfunction and eigenmode-spacing statistics in chaotic photonic crystal graphs, *Phys. Rev. E* **106**, 054215 (2022).
- [20] M. S. Ghidaoui, M. Zhao, D. A. McInnis, and D. H. Axworthy, A review of water Hammer theory and practice, *Appl. Mech. Rev.* **58**, 49 (2005).
- [21] C. C. Mei and H. Jing, Pressure and wall shear stress in blood hammer—Analytical theory, *Mathematical Biosciences* **280**, 62 (2016).
- [22] A. Barman, G. Gubbiotti, and S. E. A. Ladak, *J. Phys.: Condens. Matter* **33**, 413001 (2021).
- [23] M. Białous, P. Dulian, A. Sawicki, and L. Sirko, Delay-time distribution in the scattering of short Gaussian pulses in microwave networks, *Phys. Rev. E* **104**, 024223 (2021).
- [24] A. S. Tijsseling, Fluid-structure interaction in liquid-filled pipe systems: A review, *J. Fluids Struct.* **10**, 109 (1996).
- [25] S. Pal, P. R. Hanmaiahgari, and B. W. Karney, An overview of the numerical approaches to water hammer modelling: The ongoing quest for practical and accurate numerical approaches, *Water* **13**, 1597 (2021).
- [26] M. Brio, J. G. Caputo, and H. Kratitz, Spectral solutions of PDE's on networks, *Appl. Numer. Math.* **172**, 99 (2022).
- [27] P. Freitas, Eigenvalue asymptotics for the damped wave equation on metric graphs, *J. Diff. Equ.* **263**, 2780 (2017).
- [28] A. Bayle and F. Plouraboué, Low-mach number asymptotic analysis of Fluid-Structure-Interaction (FSI) pressure waves inside an elastic tube, *Eur. J. Mech. B* **101**, 59 (2023).
- [29] M. H. Chaudhry, *Applied Hydraulic Transients*, 3rd ed. (Springer-Verlag, Berlin, 2014).
- [30] P. Kuchment, Quantum graphs: I. Some basic structures, *Waves Random Complex Media* **14**, S107 (2004).
- [31] G. Berkolaiko and P. Kuchment, Dependence of the spectrum of a quantum graph on vertex conditions and edge length, in *Spectral Geometry Proceedings of Symposia in Pure Mathematics*, NordiCHI (American Mathematical Society, Providence, 2017), pp. 117–139.
- [32] G. Berkolaiko, J. B. Kennedy, P. Kurasov, and D. Mugnolo, Surgery principles for the spectral analysis of quantum graphs, *Trans. Amer. Math. Soc.* **372**, 5153 (2019).
- [33] A. Bayle and F. Plouraboué, Spectral properties of Fluid-Structure-Interaction pressure/stress waves in liquid filled pipes, *Wave Motion* **116**, 103081 (2023).
- [34] P. Kurasov and M. Nowaczyk, Inverse spectral problem for quantum graphs, *J. Phys. A: Math. Theor* **38**, 4901 (2005).
- [35] L. Jönsson and M. Larson, Leak detection through hydraulic transient analysis, in *Pipeline Systems* (Springer, Berlin, 1992), pp. 273–286.
- [36] X. Wang, F. Lambert, A. R. Simpson, J. A. Liggett, and J. P. Vitkovský, Leak detection in pipelines using the damping of fluid transients, *J. Hydraul. Eng.* **128**, 697 (2002).
- [37] E. J. Hinch, *Perturbation Methods*, Cambridge Texts in Applied Mathematics (Cambridge University Press, Cambridge, 1991).
- [38] C. Besse, R. Duboscq, and S. Le Coz, Numerical simulations on nonlinear quantum graphs with the GraFiDi library, *SMAI J. Comput.* **8**, 1 (2022).
- [39] A. A. Hagberg, D. A. Schult, and P. J. Swart, Exploring network structure, dynamics, and function using network, in *Proceedings of the 7th Python in Science Conference (SciPy2008)*, NordiCHI, edited by G. Varoquaux, T. Vaught, and J. Millman, Pasadena, CA USA, 2008, pp. 11–15.
- [40] See Supplemental Material at <http://link.aps.org/supplemental/10.1103/PhysRevE.109.054310> for three movies that illustrate the quantum-graph wave within a three-star metric graph, with (i.e., for water-hammer small parameter $\epsilon = 0.1, 0.01$) and without damping.